ORGANIC PROCESS RESEARCH & DEVELOPMENT
OPR&D

pubs.acs.org/OPRD

Article

# Formulation of Diacerein Cocrystal Using β-Resorcylic Acid for Improvement of Physicomechanical and Biopharmaceutical Properties

Rajeshri D. Patel* and Mihir K. Raval

Cite This: *Org. Process Res. Dev.* 2021, 25, 384−394

Read Online

ACCESS | Metrics & More | Article Recommendations | Supporting Information

**ABSTRACT:** Diacerein (DIA) is an approved treatment for osteoarthritis. However, its clinical effectiveness is limited because of its poor aqueous solubility, which causes bioavailability issues. The current study aimed to augment the functionality of DIA using a cocrystallization approach. A newly developed cocrystal of DIA with β-resorcylic acid (RA) was produced at different ratios via the antisolvent crystallization technique. Differential scanning calorimetry (DSC), powder X-ray diffraction (PXRD), Fourier transform IR (FT-IR) spectroscopy, and scanning electron microscopy (SEM) were carried out to investigate the formation of the cocrystals. The cocrystallized samples were further evaluated for their biopharmaceutical properties. The DSC study demonstrated a "W"-type phase diagram with a sharp endothermic event at a DIA:RA molar ratio of 1:3. A distinct PXRD pattern at the optimized ratio confirmed the formation of a novel cocrystal, and this was confirmed using FT-IR analysis. SEM analysis revealed the topographical variation of the prepared cocrystal, suggesting the generation of a new solid phase. Physicomechanical properties such as apparent solubility, dissolution, packability, compressibility, compactibility, and stability exhibited the improved functionality of the prepared cocrystal compared with pure DIA. Significant enhancement of bioavailability (3.2-fold) was observed for the prepared cocrystal relative to DIA alone. Hence, the fast dissolving capability and improved tabletability and bioavailability of the DIA−RA cocrystal make it a more favorable candidate for better dosage form development.

**KEYWORDS:** *diacerein, β-resorcylic acid, cocrystal, antisolvent cocrystallization, biopharmaceutical properties, physicomechanical parameters*



## 1. INTRODUCTION

Comprehensive knowledge of the solid-state properties of active pharmaceutical ingredients (APIs) plays an essential role in the pharmaceutical arena.[1] The majority of already existing APIs and new drug molecules suffer a lot of challenges in the commercialization stages because of their poor solubility, dissolution, chemical stability, moisture uptake, mechanical behaviors, manufacturability, and bioavailability, and so on.[2,3] In this context, drug candidates with desirable pharmaceutical properties are being special attention in the development of successful dosage forms especially for the pharmaceutical industry and regulatory concerns.

Various approaches such as solid dispersion, cosolvency, complexation, particle size reduction, crystal engineering, and many more have been adopted to improve the biopharmaceutical parameters that can make them suitable for the successful formulation.[4] In the current scenario, crystal engineering adopting the principle of supramolecular chemistry has attracted enormous attention from pharmaceutical scientists. This approach involves understanding the intermolecular interaction of APIs with countermolecules/coformers (CFs) and manipulating the pharmaceutically relevant properties of various APIs without compromising their efficacy.[5,6] This includes the formation of polymorphs,[7] solid solutions,[8] eutectics,[9] cocrystals,[10] solvates,[11] hydrates,[12] and coamorphous systems,[13] which can lead to improved overall functionality of APIs without changing their chemical structure. A pharmaceutical cocrystal is a crystalline adduct generated by combining an API and countermolecule/CF noncovalently in a single-crystal lattice in definite stoichiometric amounts.[14] The crystalline materials of the cocrystal differ from those of the individual participating components and could potentially exhibit better pharmaceutical behaviors.[15−18]

Diacerein (DIA), chemically known as 4,5-diacetyloxy-9,10-dioxoanthracene-2-carboxylic acid, is approved for the treatment of osteoarthritis, has mild anti-inflammatory, antipyretic, analgesic activities, and is metabolized to the diacetyl precursor Rhein.[19−21] The molecular weight of DIA is 368.3 g/mol, and the LogP is 2.4. It exists as a yellow crystalline material with a melting point of 255.2 °C. On the basis of its aqueous solubility, it is classified as a BCS II drug (~3.197 mg/L) which limits its oral absorption (35−56%).[22] Additionally, DIA shows poor processing characteristics concerning flowability, tabletability, manufacturability, and compressibility, further leading to difficulties in the development of pharmaceutical

**Special Issue:** Celebrating Women in Process Chemistry

**Received:** June 27, 2020
**Published:** October 28, 2020

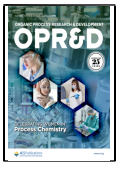

oral solid forms.[23] Several formulation approaches like solid dispersion, self-nanoemulsion, particle size reduction, nanofiber formation, complexation, and nanoparticle formation have been tried in order to tailor the pharmaceutical properties of DIA.[24−28] Until now, DIA has not been much explored in the field of crystal engineering to improve its functionality.

With this background, an attempt has been made to design a novel cocrystal of DIA with β-resorcylic acid (2,4-dihydroxybenzoic acid, RA) as a CF using the antisolvent cocrystallization technique. RA contains carboxylic acid and hydroxyl functional groups and also is regarded as a Generally Recognized as Safe (GRAS) CF that modulates the melting point of the targeted molecule effortlessly.[29] This article explains the use of the differential scanning calorimetry (DSC) technique as a diagnostic tool to assess the generation of crystalline adducts (mainly cocrystal/eutectic) and a roadmap for beginners who wish to pursue their research on multicomponent systems and their detection using DSC analysis. Finally, the resulting cocrystallized material was converted into directly compressible tablets. This study offers insight into the cocrystallization approach for simultaneous improvement of physicomechanical and biopharmaceutical parameters.

## 2. EXPERIMENTAL SECTION

**2.1. Materials.** DIA was a kind gift from Ami Lifesciences Pvt. Ltd. (Baroda, India) with batch no. DSN/40400615. RA

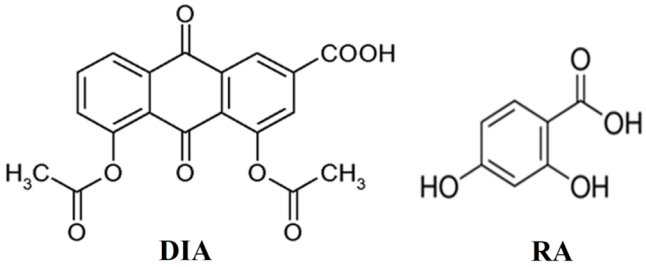


**Figure 1.** Molecular structures of diacerein (DIA) and β-resorcylic acid (RA).

**Table 1. Formulation of Directly Compressible Tablets of DIA and DIA−RA Samples**

| ingredient | amount per tablet (mg)[a] | |
|---|---|---|
| | pure drug | DIA−RA sample |
| diacerein IP | 50 | 141.4[b] |
| lactose monohydrate | 115 | 48.6 |
| microcrystalline cellulose-102 | 25 | 5 |
| Aerosil-200 | 25 | 20 |
| sodium starch glycolate | 25 | 25 |
| magnesium stearate | 5 | 5 |
| talc | 5 | 5 |

[a]Total tablet weight was 250 mg. [b]Equivalent to 50 mg of DIA.

(Sisco Research Laboratories Pvt. Ltd., Mumbai, India) and Rhein (Rh) (an active metabolite of DIA) used for formulation of the cocrystals were received from Yucca Enterprises (Mumbai, India). The molecular structures of DIA and RA are shown in Figure 1. HPLC-grade organic solvents were procured from Merck Pvt. Ltd. (Mumbai, India). AR-grade dimethyl sulfoxide (DMSO) was procured from Spectrochem Pvt. Ltd. (Mumbai, India). All of the other reagents and chemicals were used without further purification. Ultrapure water was generated in-house using a Milli-Q (Merck Millipore Pvt. Ltd., India) water purification system.

**2.2. Preparation of Multicomponent Solid Forms by the Antisolvent Cocrystallization Technique.** A saturated solution of DIA (368.3 mg, 1 mmol) in DMSO (1 volume) was prepared to make sure that DIA could be completely dissolved to obtain the organic phase. Meanwhile, the antisolvent phase was prepared by dispersing RA (462.4 mg, 3 mmol) in an excess quantity of distilled water (10 volumes). Then the organic phase was introduced slowly to the antisolvent solution at room temperature within 30 min with stirring at 200 rpm. After complete addition of the organic solution, the mixture was continuously agitated for another 2 h to allow sufficient crystal growth. The produced precipitates were then filtered and vacuum-dried at 50 °C overnight. The resulting dried product was passed through an ASTM no. 100 sieve (150 μm) and then placed in a desiccator for further study. The physical mixture of DIA and RA was obtained by geometric mixing of the individual components in the given ratio in the agate mortar and pestle immediately before use.

**2.3. Characterization Techniques.** Thermal characteristics were investigated using DSC (DSC 60, Shimadzu, Japan). The DSC samples (2−3 mg) were weighed and sealed in alumina pans. A hermetically sealed, empty alumina pan was employed as a reference. The experiments were performed at a heating rate of 5 °C/min from 40 to 300 °C under a 100 mL/min nitrogen gas flow. The data were recorded using in-built software (TA 60). Powder X-ray diffraction (PXRD) experiments were evaluated on a powder X-ray diffractometer (PANalytical, Almelo, The Netherlands) utilizing Cu Kα radiation ($\lambda$ = 1.5406 Å). The tube voltage and current were 40 kV and 30 mA, respectively. The samples were scanned between 10° and 40° ($2\theta$) with a step size of 0.0499° and a dwell time of 1 s/step. A Fourier transform infrared (FT-IR) spectrometer (Cary-630, Agilent Technologies, Cary, NC, USA) with a diamond attenuated total reflectance (ATR) accessory was used to collect the IR spectra of the samples. Samples (1−2 mg) were obtained, and their spectra were recorded from 4000 to 400 $cm^{-1}$ with a resolution of 4 $cm^{-1}$ at an accumulation of four scans. Data were analyzed using Lab Solution software (Agilent Technologies).

**2.4. Drug Content Analysis.** HPLC analysis for the quantification of DIA was performed on a Shimadzu model LC-20AD chromatograph consisting of a thermostated column (CTO-20AC), a SIL20AC autosampler, and a vacuum degasser (DGU-20A5R) and equipped with a PDA detector (SPD-M 20A). The data acquisition and processing were accomplished using the Lab Solution software (version 5.53 SP3C). The chromatographic separations were achieved on a Phenomenex Gemini C18 column (250 mm × 4.6 mm, 5 μm) with a gradient binary mobile phase consisting of acetonitrile (ACN) and ammonium acetate buffer (10 mM, pH 3.0) as given in Table S1. For the analysis of drug content (in triplicate), the obtained sample (10 mg) was weighed accurately into a 10 mL volumetric flask, dissolved in 1 mL DMSO, and exposed to ultrasound for 5 min, and the volume was completed with ACN. After appropriate dilution, the sample was subjected to HPLC analysis.

**2.5. Evaluation of Mechanical Properties.** *2.5.1. Morphological Studies.* Morphological studies of the pure components and the prepared samples were performed using scanning electron microscopy (SEM) (JSM-6380, JEOL Ltd.,


https://dx.doi.org/10.1021/acs.oprd.0c00298
Org. Process Res. Dev. 2021, 25, 384−394

Tokyo, Japan) equipped with an image analyzer. SEM was performed at an accelerating voltage of 10 kV. The powder samples (10−20 mg) were mounted on a double-sided tap and sputtered with gold. The sputter coater instrument was employed to make the sample electrically conductive. The images were recorded over the magnification range of 5000× to 10000×.

*2.5.2. Flow Characteristic.* Different micrometric parameters (angle of repose, Carr index (CI), and Hausner ratio) were determined to test the flowability of the samples. CI and Hausner ratio were derived from the bulk density and tapped density of the powder, obtained using a tapped density apparatus (ETD-1020, Electrolab, India), using eqs 1 and 2:

$$\mathrm{CI} = \frac{\text{tapped density} - \text{bulk density}}{\text{tapped density}} \times 100 \tag{1}$$

$$\text{Hausner ratio} = \frac{\text{tapped density}}{\text{bulk density}} \tag{2}$$

The angle of repose $\theta$ was determined by the fixed funnel method utilizing eq 3:[9,30]

$$\theta = \tan^{-1}\frac{h}{r} \tag{3}$$

where $h$ and $r$ are the height and radius of the pile, respectively.

*2.5.3. Powder Compaction and Compression Analysis.* The compaction and compression behavior of the compact powder were explored by performing Heckel analysis and measuring the tensile strength. The compacts (200 ± 5 mg) of pure DIA and the cocrystal samples were prepared utilizing a KBr press (Techno-search Instruments, Mumbai, India) with a 10 mm flat-faced punch. During the study, the prepared compacts were laminated immediately upon ejection from the die. This problem was resolved through the addition of a small quantity of 2% w/w microcrystalline cellulose-102 (MCC) as a binder to each sample. To understand the compaction behavior, the resulting powders were compressed under different forces ranging from 1 to 9 tons ($9.8 \times 10^3$ to $88.26 \times 10^3$ N) with a dwell time of 1 min.[31] Before the compaction process, the die and punch were lubricated using a dispersion of magnesium stearate in acetone (1% w/v).[32,33] Heckel analysis expresses the compression behavior of the powder under pressure following first-order kinetics, as shown in eq 4:

$$\ln\left[\frac{1}{(1-D)}\right] = KP + A \tag{4}$$

where $D$ is the relative density of the compact (i.e., the ratio of the compact density to the true density), $1 - D$ is the porosity ($\varepsilon$) of the powder, $P$ is the applied pressure, and $K$ (the slope) and $A$ (the $y$ intercept) are the Heckel constants calculated from the Heckel plot (a graph of $\ln[1/(1-D)]$ vs $P$). The mean yield pressure ($P_y$) is given by $K = 1/P_y$, and $A$ denotes the densification at low pressure. The yield strength ($\sigma_0$), which demonstrates the powder characteristics during deformation or fragmentation, is calculated as $\sigma_0 = (3K)^{-1}$.[9,31] Here the true densities were measured as mass per unit volume of the compact at the highest applied force in tons.[34]

After storage for 24 h, the crushing strengths and tensile strengths of the compacts were calculated as follows (eq 5):

$$T = \frac{2F}{\pi Dt} \tag{5}$$

where $T$ is the tensile strength of the compact (in N/mm$^2$), $F$ is the crushing strength of the compact (in N), and $D$ and $T$ are diameter (in mm) and thickness (in mm) of the compact, respectively, all of which were calculated using a Mitutoyo vernier caliper. In separate experiments, the compression behaviors of novel solid forms were examined by the Aulton−Wells method.[35] Each 200 mg sample was blended with 1% magnesium stearate and 2% MCC in a glass vial, and the mixture was processed according to the compression protocol given in Table S2. The crushing strengths of the compacts formed were evaluated using a digital hardness tester (Electrolab Pvt. Ltd., India) after equilibration for 24 h.

**2.6. Preparation and Evaluation Parameters of Directly Compressible Tablets.** Tablets comprising 250 mg equivalent to DIA (tablets of pure DIA and DIA−RA samples) were formulated using the direct compression technique with different formulation excipients as listed in Table 1. The appropriate quantities of sieved pure DIA and DIA−RA sample were mixed separately with the described amounts of other ingredients to prepare nearly 40 tablets from each batch. The material for each tablet was manually added into the die and compressed in the tablet machine (Karnawati Engineering Ltd., India) using a 12 mm round and concave-shaped punch. The tablets were prepared and kept in airtight bottles for 24 h before use to attain suitable elastic recovery and hardness. The compressed tablets were then evaluated for weight variation, tablet strength, friability, and disintegrated time measurements. The tablet strength was determined using a digital hardness tester, and the friability was measured as the percent mass loss of 20 tablets tumbled in a Roche friabilator (EF-2, Electrolab Pvt. Ltd., India). Disintegration time ($T_D$) measurements (ED2, Electrolab Pvt. Ltd., India) were performed on six tablets in 900 mL of distilled water at 37 ± 1 °C as described in the Indian Pharmacopoeia 2010.[36]

**2.7. Apparent Solubility Study.** Apparent solubility measurements on DIA, the prepared samples, and their physical mixture were performed by equilibrating an excess amount of drug (equivalent to 50 mg of DIA) in 10 mL of various buffer preparations in triplicate, especially distilled water, hydrochloric acid buffer (pH 1.2), acetate buffer (pH 4.5), and phosphate buffer (pH 6.8) using the shake flask method. An incubator shaker (Tempo Instruments and Equipment Pvt. Ltd., India) was used to keep the samples at 150 rpm for 24 h at 37 ± 0.5 °C. After this period, the resulting samples were immediately filtered using a PVDF syringe filter (0.45 $\mu$m), suitably diluted with the corresponding media, and analyzed by the validated RP-HPLC method.

**2.8. In Vitro Dissolution Study.** A drug dissolution study was evaluated using a USP type-II apparatus (TDT-06P, Electrolab, India). Commercial DIA tablets, Lubry-GM (50 mg) as a reference, and prepared cocrystal tablets were added to 900 mL of citrate buffer (pH 6) as a dissolution medium equilibrated at 37 ± 0.5 °C at 75 rpm.[36] Aliquots (5 mL each) were withdrawn (with replacement by fresh buffer) at predefined intervals. The concentrations of the aliquots were estimated using the developed reversed-phase (RP) HPLC method with appropriate dilutions (wherever necessary). The dissolution profiles were analyzed in terms of model-independent parameters calculated at different time intervals,


https://dx.doi.org/10.1021/acs.oprd.0c00298
Org. Process Res. Dev. 2021, 25, 384−394

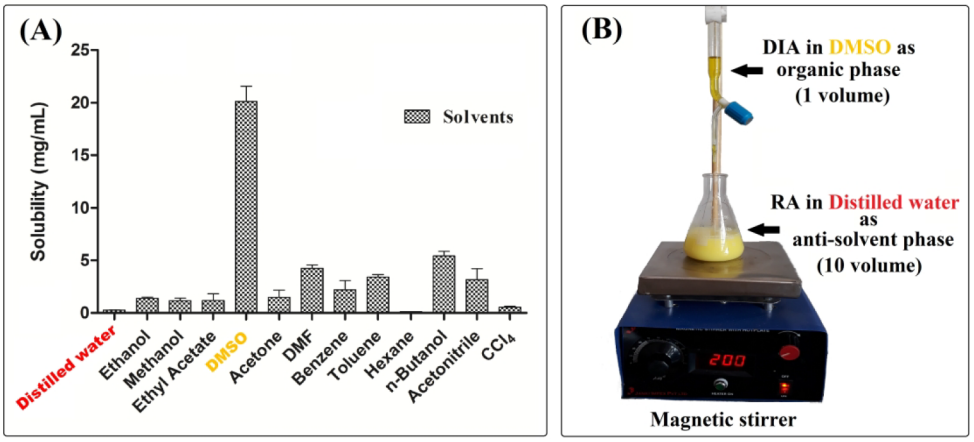


**Figure 2.** (A) Solubility assessment of DIA in various solvents and (B) experimental setup for antisolvent cocrystallization.

such as percent dissolution at 5 min ($\%DP_{5\ min}$), dissolution efficiency ($\%DE_{10\ min}$), $MDT_{in\ vitro}$, and similarity factor ($f_2$).[37]

**2.9. Pharmacokinetic Study.** The in vivo pharmacokinetic study was performed using healthy Sprague-Dawley rats (either sex). The Institutional Animal Ethics Committee (IAEC) approved the experimental protocol (IAEC/DPS/SU/1609; dated December 12, 2016). All of the animals (~250 g) were housed in the polypropylene cages and kept at 25 ± 2 °C and 50−60% relative humidity (RH). The animals were acclimatized for a week and subsequently fasted overnight with free access to water before the experiment. Twenty-four rats were randomly distributed in two groups (12 rats in each group) and orally administered with a single dose of DIA or prepared sample, respectively. The raw DIA and prepared sample were suspended in 0.2% w/v sodium carboxymethylcellulose and administered through oral gavage. Each animal was treated with a DIA dose equivalent to 30 mg/kg of body weight, respectively.[31,38] Blood samples were collected from the retro-orbital venous plexus of the rats at different time points (0, 0.25, 0.5, 0.75, 1, 1.5, 2, 4, 6, 12, and 24 h). The plasma samples were harvested by centrifugation at 10 000 rpm for 20 min and frozen at −20 °C until determination; see section S1 in the Supporting Information (SI) for the plasma sample preparation and method. Pharmacokinetic parameters such as area under the curve (AUC), area under the plasma concentration−time curve ($AUC_{0-t}$), area under the moment curve (AUMC), time to maximum concentration ($T_{max}$), maximum plasma concentration ($C_{max}$), total clearance (CL), mean residence time (MRT), volume of distribution ($V_D$), and elimination half-life ($T_{1/2}$) were calculated using PK Solver 2 (Microsoft Excel add-in program).

**2.10. Stability Study.** The stability study was performed on DIA−RA cocrystal samples (powder as well as tablet) stored at 40 °C and 75% RH in a programmable environmental test chamber (Remi SC-16 PLUS, India) for 6 months. The dissolution profiles of the powder and tablet formulations were evaluated, and the integrity of the samples was analyzed by DSC, FT-IR, and PXRD analyses.

**2.11. Statistical Analysis.** GraphPad Prism 5.0 (GraphPad Software, Inc., San Diego, CA, USA) was used to perform the statistical data analysis. A level of $p < 0.05$ was used to indicate statistical significance in all cases. The data were analyzed as mean ± standard deviation (SD).

## 3. RESULTS AND DISCUSSION

DIA is an enthralling drug molecule containing potential functional groups like −COOH, −C−O−C−, and −COOC−,

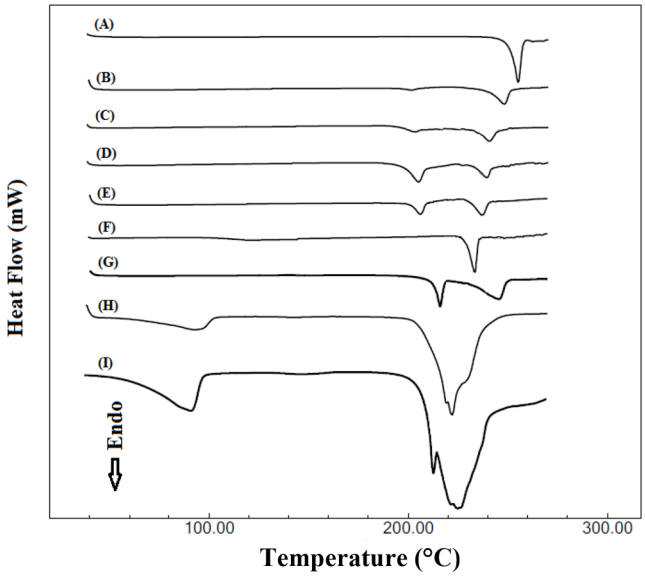


**Figure 3.** DSC endotherms of (A) pure DIA, (B−G) the DIA−RA system prepared by the antisolvent cocrystallization method at various DIA:RA molar ratios (B, 3:1; C, 2:1; D, 1:1; E, 1:2; F, 1:3; G, 1:4), (H) pure RA, and (I) a physical mixture of DIA−RA system in a 1:3 molar ratio.

which have a significant role in the field of crystal engineering. In the previous research on cocrystallization of DIA, the practical use of mechanochemical methods has received special attention.[39,40] Additionally, our previous research obtained a newly developed eutectic between DIA and RA (1:3) via the liquid-assisted grinding method.[31] According to the previous research, the possibility of antisolvent cocrystallization to design cocrystals is worthy of discussion.[41] Following these observations, antisolvent cocrystallization was carried out using DIA and RA as a model system for evidence of cocrystal formation for functionality improvement.

Various process parameters such as the solvent/antisolvent ratio, stirring speed, drug solution flow rate, and drug/CF concentration were screened and evaluated. The solubility assessment in various solvents (Figure 2A) and the


https://dx.doi.org/10.1021/acs.oprd.0c00298
Org. Process Res. Dev. 2021, 25, 384−394

**Table 2. Solidus and Liquidus Temperatures, Melting Points of the Pure Components ($T_m$), and $\Delta H_{fus}$ Values for the Binary Phase Diagram**[a]

| $X_{DIA}$ | $T_{solidus}$ (°C) | $T_{liquidus}$ (°C) | $T_m$ (°C) | $\Delta H_{fus}$ of DIA (J/g) |
|---|---|---|---|---|
| 1.00 | – | – | 255.17 | 96.68 |
| 0.75 | 198.79 | 251.65 | | 64.45 |
| 0.67 | 199.83 | 245.07 | | 60.69 |
| 0.50 | 200.04 | 243.22 | | 51.45 |
| 0.33 | 201.52 | 241.01 | | 46.93 |
| 0.25 | 236.16 | 237.65 | | 128.79 |
| 0.20 | 212.37 | 243.80 | | 80.46 |
| 0.00 | – | – | 222.05 | 598.80 |

[a] $X_{DIA}$, mole fraction of DIA; $T_{solidus}$, solidus temperature; $T_{liquidus}$, liquidus temperature; $T_m$, melting temperature; $\Delta H_{fus}$, heat of fusion obtained from DSC heating runs of mixtures of DIA and RA.

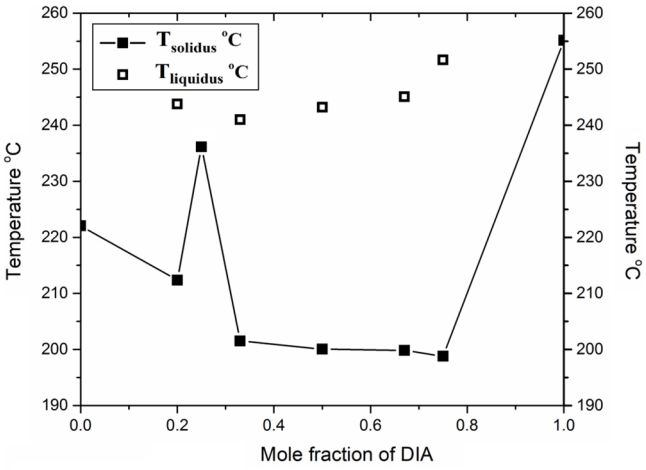


**Figure 4.** Binary phase diagram for the DIA−RA system exhibiting a "W"-type pattern characteristic of a cocrystal. The solidus and liquidus temperatures are shown with solid and open squares, respectively.

experimental setup for antisolvent cocrystallization (Figure 2B) are described in Figure 2 and SI section S2. In context to this, DMSO and distilled water were chosen as the solvent and antisolvent, respectively. The optimum volume ratio of solvent to antisolvent was selected as 1:10. The resulting materials were subjected to various characterization studies such as DSC, PXRD, and FT-IR analyses to identify the possible solid-state interaction of DIA and RA.

**3.1. Characterization.** *3.1.1. DSC Study.* DSC scans of pure drug (Figure 3A) confirmed a single melting endotherm at 255.17 °C with a corresponding endothermal effect ($\Delta H_{fus}$ = 96.68 J/g) imparting its crystalline form.[26] The melting endotherm of RA (Figure 3H) was observed as a broad peak with a melting point at 222.05 °C ($\Delta H_{fus}$ = 598.80 J/g). For the cocrystallized material with a DIA:RA molar ratio of 1:3, a single sharp endothermic peak was observed at 236.16 °C ($\Delta H_{fus}$ = 128.79 J/g) that appeared different from those of the parent compounds (Figure 3F). This melting endotherm of the cocrystallized material was between the melting endotherms of the drug and CF, indicating the existence of a new crystalline phase. Additional mixtures of DIA and RA were prepared via the antisolvent cocrystallization technique as described in section 2.2 to verify the formation of the cocrystal. However, the mixtures with DIA:RA molar ratios of 3:1 (Figure 3B), 2:1 (Figure 3C), 1:1 (Figure 3D), 1:2 (Figure 3E), and 1:4 (Figure 3G) and the physical mixture with a 1:3 molar ratio (Figure 3I) exhibited two distinct endothermic events, thereby indicating the absence of cocrystal formation (Figure 3). In a cocrystallization screening, when the system shows higher or intermediate endothermic behavior compared with the participating components, this can be accomplished with the formation of a cocrystal (although there are some exceptions). A binary phase diagram can be exploited to comprehend the distinct thermal phase transitions for the given system as a function of temperature. Table 2 presents the various solidus and liquidus temperatures and melting points of the participating compounds and $\Delta H_{fus}$ values with their molar ratios. All of the points representing the solidus events were joined to plot the temperature−composition phase diagram (dark line). The resulting diagram (Figure 4) exhibited a "W"-type pattern, which could be a characteristic of the cocrystal formation. Moreover, the middle line of the W shape was again extrapolated to the $X$ axis and crossed it at the molar ratio of 1:3.[42−44]

*3.1.2. PXRD Study.* Figure 5 illustrates the PXRD patterns of pure DIA, pure RA, the DIA−RA physical mixture, and the DIA−RA system. DIA (Figure 5A) showed characteristic peaks at 2$\theta$ values of 10.4°, 17.4°, and 27.9°.[45] RA (Figure 5B) revealed the characteristic intense peaks at 2$\theta$ values of 13.5°, 26.8°, and 28.4°.[31] The appearance of a new and distinct diffraction pattern with peaks at 2$\theta$ values at 12.2°, 18.5°, and 19.9° with decreased intensity were observed in the DIA−RA system. Also, a few peaks got shifted considerably from their positions with 2$\theta$ values of 11.0°, 22.2°, 26.1°, and 27.0°. All of the characteristic peaks are marked with stars (★) in Figure 5D. The emergence of a distinct diffraction pattern correlates the results of the DSC analysis, confirming the generation of the new cocrystal solid phase.[43,44] Additionally, all of the distinct peaks of the DIA−RA system with lower intensity compared with those of the participating components indicated a great reduction in its crystallinity.[46]

*3.1.3. FT-IR Analysis.* FT-IR spectra of DIA, RA, the DIA−RA physical mixture, and the DIA−RA system are depicted in Figure 6. DIA (Figure 6A) displayed a broad −OH stretch at 3069 $cm^{-1}$ and two C═O stretches at 1785 and 1679 $cm^{-1}$ for the acetoxy groups. For RA (Figure 6B), the broad stretch for the −OH group was observed at 2900−3600 $cm^{-1}$, and the peak for the C═O functional group appeared at 1790 $cm^{-1}$. In the FT-IR spectrum of the DIA−RA system (Figure 6D), significant peak changes were observed with respect to the positions of the carbonyl groups of the ester and ketone moieties of DIA along with the carboxylic acid group of RA. The acetoxy group −C═O (1785 $cm^{-1}$) of DIA and the carboxylic −C═O (1650 $cm^{-1}$) stretch in RA were shifted to lower wavenumbers at 1757 and 1633 $cm^{-1}$, respectively (marked with arrows in Figure 6D). This deviation in peaks suggested the possibility of hydrogen bond formation.[47] The results of the FT-IR study of the DIA−RA system (i.e., at a 1:3 molar ratio) were in agreement with the outcomes obtained from the DSC and PXRD studies, indicating the formation of the cocrystal.[43,44]

**3.2. Drug Content Analysis.** DIA exhibits pH-dependent solubility because of its weakly acidic nature. The buffer solutions having pH > 5 show the estimation of DIA in the form of Rh.[21,31] A new RP-HPLC method for the quantification of DIA and Rh was developed and validated as per ICH guideline Q2 (R1).[48] The HPLC chromatogram of the resolved mixture of RA, DIA, and Rh shows retention times


https://dx.doi.org/10.1021/acs.oprd.0c00298
Org. Process Res. Dev. 2021, 25, 384−394

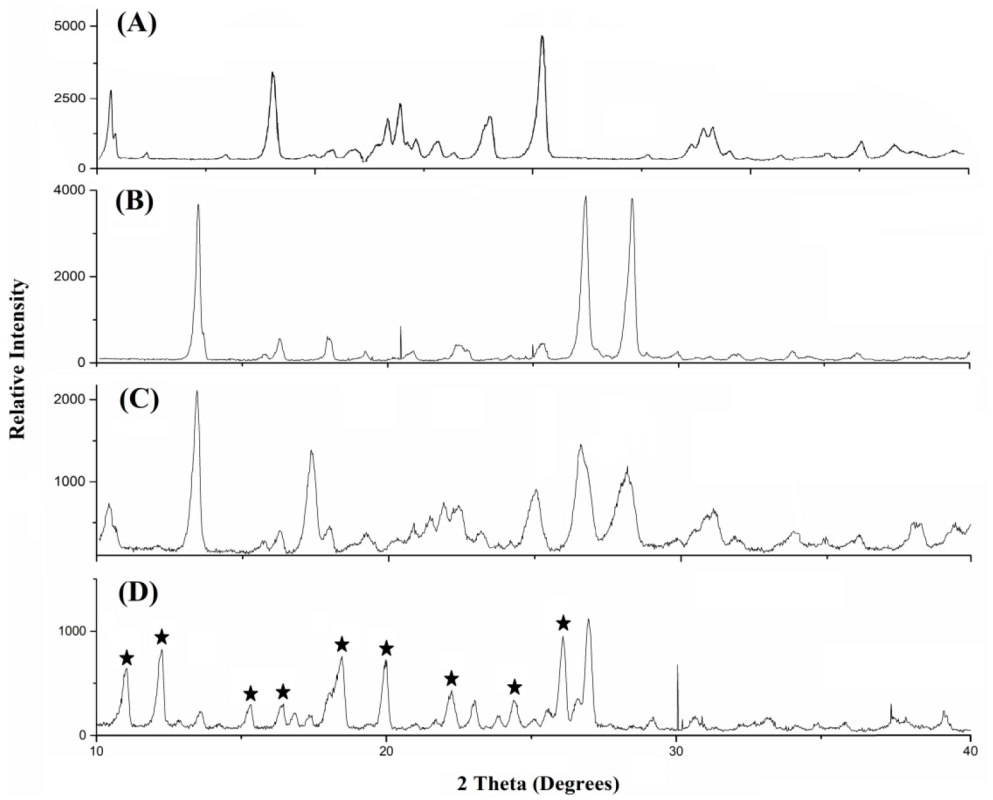


**Figure 5.** PXRD patterns of (A) DIA, (B) RA, (C) the DIA−RA physical mixture, and (D) the DIA−RA cocrystal.

($t_R$) of 6.6, 10.5, and 11.6 min, respectively (Figure S1). The detailed description of RP-HPLC conditions is explained in Table S3. The achieved method was applicable to the quantification of DIA and Rh in the prepared formulation. The drug content determination of the DIA−RA cocrystal was found to be 81.67 ± 2.43%.

**3.3. Evaluation of Mechanical Properties.** *3.3.1. Morphological Study.* The SEM images explained the surface morphology, which significantly affected the physicomechanical and pharmacokinetic parameters of the drug material. Figure 7 presents SEM images of DIA, RA, and the DIA−RA system. The SEM images of DIA (Figure 7A) showed acicular-shaped crystals with an irregular surface, which might hinder their flow and compression behavior. The SEM image of RA (Figure 7B) revealed regular and smooth-shaped crystals. The surfaces of the cocrystallized sample (Figure 7C) appeared comparatively smooth, and aggregation was good compared with the parent DIA. The morphological difference in the newly generated cocrystal could influence physicomechanical parameters such as flowability, compressibility, solubility, and dissolution, which might be beneficial for the formulation of oral solids.[49]

*3.3.2. Flow Characterization.* Various flow parameters, such as the CI, Hausner ratio, and angle of repose, were measured to evaluate the flowability of raw DIA and the cocrystal sample. The results are given in Table 3. The CI, Hausner ratio, and angle of repose of the cocrystal were found to be 29.8 ± 1.6, 1.31 ± 0.06, and 35.7° ± 1.0°, respectively. These results suggested that the cocrystal has relatively fair to good flow characteristics compared with pure DIA. It has been noted that powder flow can be influenced by several aspects like the size and morphology of the particles, size distribution, surface energy, surface texture, moisture content, etc.[50] Additionally, the CI and Hausner ratio do not express the complete flow behavior of powder. Certainly, some materials display high values of the CI and Hausner ratio but present poor flowability. However, they may consolidate quickly, which is the sign corresponding to the uniform die-fill process.[51] However, the bulk and tapped densities of the cocrystal sample were lower than the corresponding values for the pure drug. The lower density is associated with the intraparticle porosity or density,[52] and hence, the cocrystal powder showed a reduction in bulk density imparting its greater porosity within the powder materials. Therefore, the prepared cocrystal was further analyzed in terms of other mechanical parameters such as compaction and compressibility studies.

*3.3.3. Powder Compaction and Compression Analysis.* It was found that the true densities of pure DIA and the DIA−RA cocrystal were 1.0620 ± 0.04 and 1.7042 ± 0.05 g/cm$^3$, respectively. The true density values expressed that the prepared cocrystal was relatively denser than DIA alone. This variation in the true density indicated the improvement in the compression behavior of the cocrystal compared with the DIA sample. According to the Heckel plot, the derived parameters were calculated from linear regression of the straight-line plots ($R^2$ > 0.98) as shown in Figure 8A and listed in Table 3. The larger values of $K$ and $A$ in the case of the cocrystal sample compared with DIA are attributed to greater plastic behavior and particle rearrangement, whereas the lower $\sigma_0$ and $P_y$ values for the cocrystal over the pure drug are indicative of better compression behavior. Furthermore, DIA demonstrated a low brittleness index, reflecting its poor fragmentation behavior. This might be a reason for the appearance of lamination during the Heckel analysis.[31] This could be overcome by the addition of 2% w/w MCC to all of the samples followed by Heckel


https://dx.doi.org/10.1021/acs.oprd.0c00298
Org. Process Res. Dev. 2021, 25, 384−394

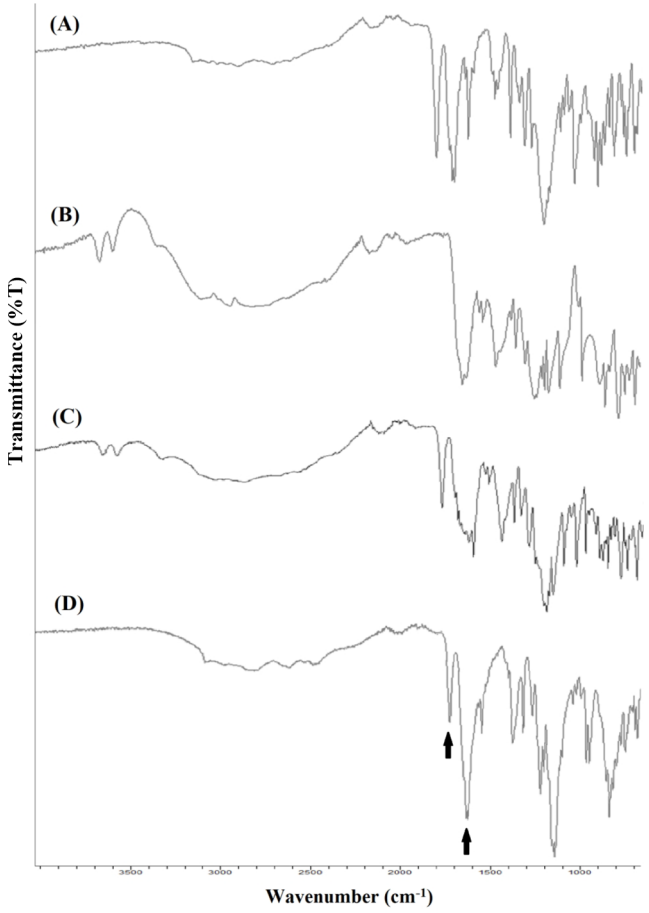


**Figure 6.** FT-IR spectra of (A) DIA, (B) RA, (C) the DIA−RA physical mixture, and (D) the DIA−RA cocrystal.

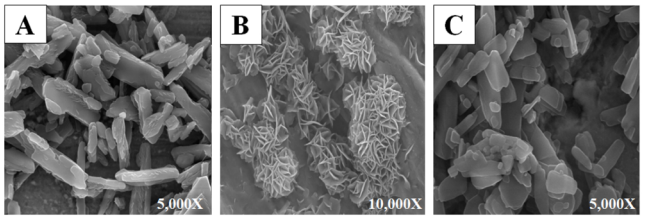


**Figure 7.** SEM images of (A) DIA, (B) RA, and (C) the DIA−RA cocrystal.

**Table 3. Evaluation of the Mechanical Properties of Pure DIA and DIA−RA Cocrystal**

| parameter | pure DIA | DIA−RA cocrystal |
|---|---|---|
| density(g/cm$^3$)[a] | | |
| bulk | 0.309 ± 0.01 | 0.139 ± 0.02 |
| tapped | 0.456 ± 0.05 | 0.199 ± 0.07 |
| true | 1.0620 ± 0.04 | 1.7042 ± 0.05 |
| angle of repose (deg)[a] | 47.1 ± 1.2 | 35.7 ± 1.0 |
| Carr index[a] | 32.2 ± 1.9 | 29.8 ± 1.6 |
| Hausner ratio[a] | 1.48 ± 0.08 | 1.31 ± 0.06 |
| Heckel analysis | | |
| $K$ | 0.161 | 0.460 |
| $A$ | 0.986 | 1.301 |
| $P_y$ | 6.212 | 2.174 |
| $\sigma_0$ | 2.070 | 0.725 |

[a]Results are mean ± SD ($n$ = 3).

analysis at different compression forces.[31,33] The pressure−tensile strength profiles of all of the samples are represented by their powder tabletability behaviors. Figure 8B illustrates that higher tensile strength was detected for compacts of the cocrystal over those of pure DIA at all applied compression forces. This was attributed to the improved compressibility and tabletability of the DIA−RA cocrystal over pure DIA.[52] Moreover, three different compacts (A, B, and C) were prepared as per the Aulton−Wells protocol to understand the in-depth compressibility of the powders. As can be seen in Figure 9, the drug compacts exhibited capping and lamination tendencies. This type of tendency despite the change in blending and dwell time is an indication of the elastic nature of the drug. In the case of the cocrystallized sample, capping and lamination were not observed, and the crushing strength measurement was in order B > A > C, which exemplified its plastic behavior. This study clearly concluded that the superior compaction and compression behaviors of the DIA−RA cocrystal compared with DIA might be due to the occurrence of interparticulate bonding in the cocrystal material, and it could be suitable as a directly compressible material.[35]

**3.4. Postevaluation Parameters of Directly Compressible Tablets.** As can be seen in Table 1, the tablets prepared from the cocrystal sample contained a smaller amount of MCC (2% w/w). This result revealed that the cocrystal of DIA could be advantageous for the development of a directly compressible form. The post evaluations are summarized in Table 4.[49]

**3.5. Apparent Solubility Study.** Solubility measurement is a significant parameter in formulation development that directly impacts the oral solid dosage form. Figure 10A depicts the graphical solubility assessment for DIA, the DIA−RA cocrystal, and the DIA/RA physical mixture in various buffer solutions. The solubility profiles of the pure drug in distilled water, pH 1.2, pH 4.5, and pH 6.8 were found to be 48.3, 9.1, 15.3, and 83.7 $\mu$g/mL, respectively. These outcomes revealed that DIA showed poor solubility in acidic buffer solutions because of its weakly acidic nature. The DIA−RA cocrystal demonstrated an enhancement in solubility of nearly 2.3 times at pH 6.8 (192 $\mu$g/mL), 2.5 times at pH 4.5 (37 $\mu$g/mL), 2.8 times at pH 1.2 (26 $\mu$g/mL), and 2.6 times in distilled water (125 $\mu$g/mL) compared with raw DIA. As can be seen from the pH solubility profiles, the DIA−RA cocrystal showed overall higher solubility than the physical mixture vis-à-vis the drug alone in all buffer solutions. Mainly, the solubility of the cocrystal depends on the solubility of the CF, the melting point, and the crystal lattice. The augmentation in solubility might be ascribed to the formation of non-covalent bonds between a poorly soluble API and highly soluble CF in the same crystal lattice.[53]

**3.6. In Vitro Dissolution Study.** The quantitative key findings explaining the dissolution profiles of the prepared cocrystal and the commercial tablet formulations at pH 6 are summarized in Table 4. The cocrystallized tablets exhibited superior drug release (83.32%) over the commercially available tablets (34.40%) after 1 h (Figure 10B). The %$DP_{5\ min}$ of the cocrystal tablets was found to be enhanced 3.3-fold compared with commercial tablets. Also, a 2.9-fold improvement in %$DE_{10\ min}$ and a lower value of MDT for the cocrystal impart its fasted dissolution capability relative to the pure DIA formulation. Furthermore, the obtained $f_2$ value was less than 50, which revealed the difference between the release profiles of the pure drug and the cocrystal (tablet formulations). This enhancement might be due to the


https://dx.doi.org/10.1021/acs.oprd.0c00298
Org. Process Res. Dev. 2021, 25, 384−394

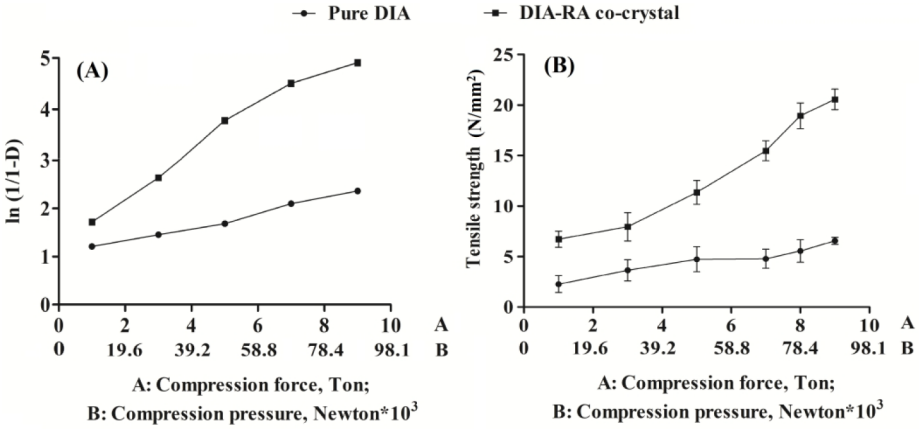


**Figure 8.** (A) Heckel plot and (B) tabletability study of pure DIA and the DIA−RA cocrystal.

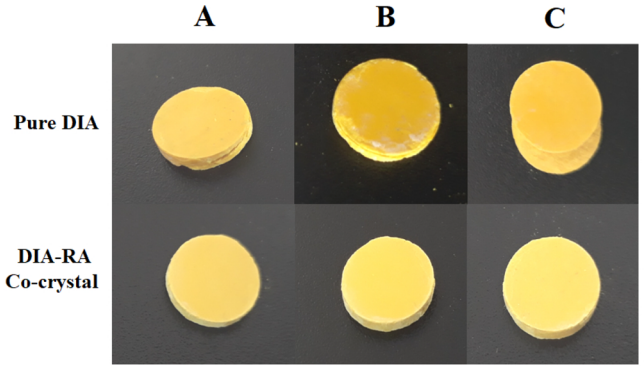


**Figure 9.** Pictorial comparison of compacts prepared from pure DIA and the DIA−RA cocrystal as per the Aulton−Wells protocol.

**Table 4. Post Evaluation and Dissolution Parameters of Direct Compression Tablets of DIA and the DIA−RA Cocrystal**

| parameter | pure DIA | DIA−RA cocrystal |
|---|---|---|
| weight variation (mg)[a] | 250.2 ± 2.43 | 249.7 ± 2.18 |
| thickness (mm)[a] | 3.39 ± 0.07 | 3.38 ± 0.05 |
| hardness (kg/cm$^2$)[a] | 4.9 ± 0.31 | 5.3 ± 0.62 |
| friability (% loss)[a] | 0.36 ± 0.08 | 0.33 ± 0.06 |
| $T_D$ (s)[a] | 65.33 ± 2.52 | 59.24 ± 2.08 |
| $\%DP_{S\ min}$[b] | 14.07 | 45.82[c] |
| $\%DE_{10\ min}$[b] | 9.12 | 26.59[c] |
| $f_2$[b] | – | 24.87 |
| MDT (min)[b] | 14.44 | 9.85 |

[a]Results are mean ± SD ($n$ = 3). [b]Calculated on the basis of tablet formulations. [c]Implies $p < 0.05$ compared with pure DIA.

hydrophilic CF (RA), which facilitates the local solubilization effects. Additionally, melting point changes indicate modification of the thermodynamic characteristics such as molecular mobility, intermolecular interaction, and crystal packing.[53,54]

**3.7. Pharmacokinetic Study.** After the improvement in solubility and dissolution parameters, the cocrystal developed in this work should furthermore be suitable for in vivo assessment using rats as a model. The plasma concentration profiles of raw drug and cocrystallized sample after a single-dose oral administration in Sprague-Dawley rats are given in Figure 11, and the calculated pharmacokinetic parameters are stated in Table 5. Because of the metabolic change from DIA to Rh, only Rh was estimated in the plasma samples to assess the in vivo performance.[31] The cocrystallized sample exhibited a shortened $T_{max}$ (2 h) with an increase in $C_{max}$ (92.68 μg/mL) compared with raw DIA. The $AUC_{0-24h}$ (total drug delivered in 24 h) was 650.1 μg·h/mL for the cocrystal compared with 249.9 μg·h/mL for DIA alone (it is transformed to Rh in vivo). Furthermore, the relative bioavailability ($F_{rel}$), given by the ratio of the $AUC_{total}$(cocrystal) to $AUC_{total}$ (drug), was found to be 2.28. This outcome demonstrated that the DIA−RA cocrystal was 2.28-fold more orally bioavailable than DIA.[55] This finding suggested that the cocrystallization of DIA in the presence of RA is an advantage in the biopharmaceutical properties of the parent DIA.

**3.8. Stability Study.** A stability study of the cocrystallized samples (powder as well as tablet) was performed under accelerated conditions for 6 months. The dissolution profiles of the cocrystal (powder and tablet) before and after the study (Figure S2) were similar, as represented statistically by $f_2 > 50$. Similar results were also found in the case of DSC, FT-IR, and PXRD data before and after 6 months, indicating that the cocrystal samples were stable in nature (Figures S3−S5).

## 4. CONCLUSION

DIA is a potential osteoarthritis agent that has poor biopharmaceutical properties. In this work, a novel DIA−RA cocrystal (DIA:RA molar ratio = 1:3) was obtained using the antisolvent crystallization technique and fully characterized. The prepared cocrystal was evaluated for pharmacomechanical parameters such as apparent solubility, dissolution, powder characteristics, and stability. Significant enhancement in the aforementioned properties was observed in the DIA−RA cocrystal compared with raw DIA. Furthermore, the novel cocrystal showed better plastic behavior and tabletability characteristics compared with pure DIA, enabling its formulation as a directly compressible tablet. The DIA−RA cocrystal also showed a notable improvement in oral bioavailability. Unfortunately, we did not succeed in structural elucidation of the cocrystal using crystallographic techniques, which will be necessary to explore for further understanding the solid-state interaction. In a nutshell, the cocrystallization approach can be applied to the pharmaceutical industry to address poorly compressible and bioavailable APIs to convert them to forms suitable for direct compression.


https://dx.doi.org/10.1021/acs.oprd.0c00298
Org. Process Res. Dev. 2021, 25, 384−394

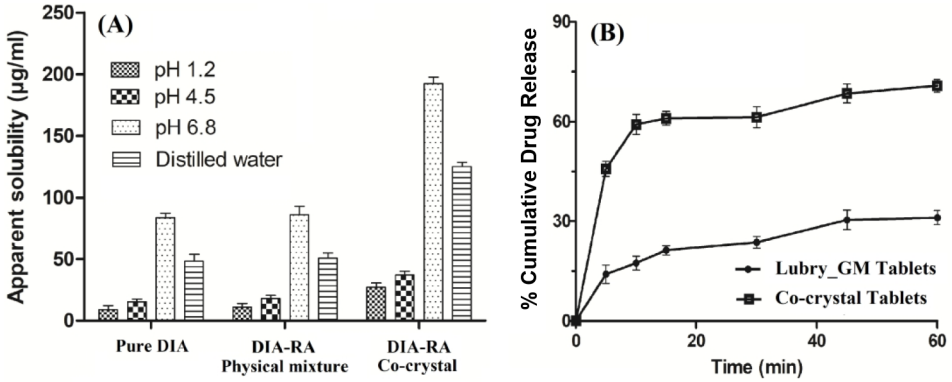


**Figure 10.** (A) Apparent solubility measurements on pure DIA, the DIA/RA physical mixture, and the DIA−RA cocrystal at pH 1.2, pH 4.5, and pH 6.8 and in distilled water. (B) In vitro drug release profiles of pure DIA and DIA−RA cocrystal tablets.

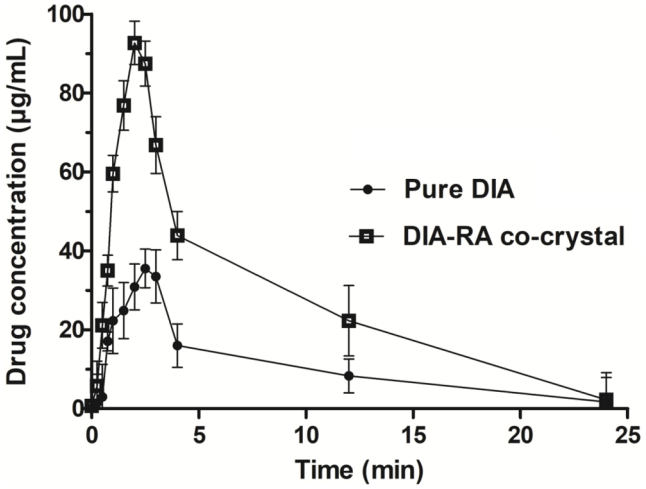


**Figure 11.** Mean plasma concentration−time curves for DIA and the DIA−RA cocrystal.

**Table 5. Pharmacokinetic Parameters of DIA and the DIA−RA Cocrystal after Single Oral Dose Administration to Sprague-Dawley Rats**[a]

| parameter | DIA | DIA−RA cocrystal |
|---|---|---|
| $C_{max}$ (μg/mL) | 35.54 ± 5.72 | 92.68 ± 4.29 |
| $T_{max}$ (h) | 2.5 ± 0.92 | 2.0 ± 0.79 |
| $AUC_{0-24h}$ (μg·h/mL) | 249.91 ± 152.43 | 650.08 ± 116.26 |
| $AUC_{total}$ (μg·h/mL) | 298.60 ± 141.19 | 682.35 ± 185.32 |
| $F_{rel}$ | 1 | 2.28 |

[a]Results are mean ± SD ($n$ = 6).

## ■ ASSOCIATED CONTENT

### Supporting Information

The Supporting Information is available free of charge at https://pubs.acs.org/doi/10.1021/acs.oprd.0c00298.

Plasma sample preparation and method (S1); solvent selection for optimization of the antisolvent method (S2); gradient system for the developed RP-HPLC method (Table S1); Aulton−Wells compression protocol (Table S2); chromatographic parameters (Table S3); representative HPLC chromatogram for the DIA−RA system (Figure S1); dissolution profiles for powder and tablet forms (Figure S2); DSC analysis (Figure S3); PXRD data (Figure S4); FT-IR data before and after reaching stability conditions (Figure S5) (PDF)

## ■ AUTHOR INFORMATION


### Corresponding Author

**Rajeshri D. Patel** − *Department of Pharmaceutical Sciences, Saurashtra University, Rajkot 360 005, Gujarat, India;* orcid.org/0000-0001-9824-2494; Email: rajeshripatel.2504@gmail.com

### Author

**Mihir K. Raval** − *Department of Pharmaceutical Sciences, Saurashtra University, Rajkot 360 005, Gujarat, India*

Complete contact information is available at: https://pubs.acs.org/10.1021/acs.oprd.0c00298


### Notes

The authors declare no competing financial interest.

## ■ ACKNOWLEDGMENTS

R.D.P. acknowledges the Department of Science and Technology (DST), New Delhi, India, for providing Inspire Fellowship vide letter number DST/INSPIRE Fellowship/2013/1079.

## ■ REFERENCES


(1) Stegemann, S.; Leveiller, F.; Franchi, D.; De Jong, H.; Lindén, H. When poor solubility becomes an issue: from early stage to proof of concept. *Eur. J. Pharm. Sci.* **2007**, *31*, 249−246.

(2) Sun, C. C. Cocrystallization for successful drug delivery. *Expert Opin. Drug Delivery* **2013**, *10*, 201−213.

(3) Gardner, C. R.; Walsh, C. T.; Almarsson, Ö. Drugs as materials: valuing physical form in drug discovery. *Nat. Rev. Drug Discovery* **2004**, *3*, 926−934.

(4) Avdeef, A. Physicochemical profiling (solubility, permeability and charge state). *Curr. Top. Med. Chem.* **2001**, *1*, 277−351.

(5) Desiraju, G. R. Supramolecular synthons in crystal engineering—a new organic synthesis. *Angew. Chem., Int. Ed. Engl.* **1995**, *34*, 2311−2327.

(6) Desiraju, G. R. Crystal engineering: from molecule to crystal. *J. Am. Chem. Soc.* **2013**, *135*, 9952−9967.

(7) Lancaster, R. W.; Karamertzanis, P. G.; Hulme, A. T.; Tocher, D. A.; Lewis, T. C.; Price, S. L. The polymorphism of progesterone: Stabilization of a 'disappearing' polymorph by co-crystallization. *J. Pharm. Sci.* **2007**, *96*, 3419−3431.

(8) Chakraborty, S.; Desiraju, G. R. C−H···F Hydrogen Bonds in Solid Solutions of Benzoic Acid and 4-Fluorobenzoic acid. *Cryst. Growth Des.* **2018**, *18*, 3607−3615.

(9) Patel, R. D.; Raval, M. K.; Bagathariya, A. A.; Sheth, N. R. Functionality improvement of Nimesulide by eutectic formation with

nicotinamide: Exploration using temperature-composition phase diagram. *Adv. Powder Technol.* **2019**, *30*, 961−973.
(10) Ren, S.; Liu, M.; Hong, C.; Li, G.; Sun, J.; Wang, J.; Zhang, L.; Xie, Y. The effects of pH, surfactant, ion concentration, coformer, and molecular arrangement on the solubility behavior of myricetin cocrystals. *Acta Pharm. Sin. B* **2019**, *9*, 59−73.
(11) Van Tonder, E. C.; Mahlatji, M. D.; Malan, S. F.; Liebenberg, W.; Caira, M. R.; Song, M.; De Villiers, M. M. Preparation and physicochemical characterization of 5 niclosamide solvates and 1 hemisolvate. *AAPS PharmSciTech* **2004**, *5*, 86.
(12) Giron, D.; Goldbronn, C.; Mutz, M.; Pfeffer, S.; Piechon, P.; Schwab, P. Solid state characterizations of pharmaceutical hydrates. *J. Therm. Anal. Calorim.* **2002**, *68*, 453−465.
(13) Suresh, K.; Mannava, M. C.; Nangia, A. A novel curcumin-artemisinin coamorphous solid: Physical properties and pharmacokinetic profile. *RSC Adv.* **2014**, *4*, 58357−58361.
(14) Duggirala, N. K.; Perry, M. L.; Almarsson, Ö.; Zaworotko, M. J. Pharmaceutical cocrystals: along the path to improved medicines. *Chem. Commun.* **2016**, *52*, 640−655.
(15) Bolla, G.; Nangia, A. Pharmaceutical cocrystals: walking the talk. *Chem. Commun.* **2016**, *52*, 8342−8360.
(16) Cerreia Vioglio, P.; Chierotti, M. R.; Gobetto, R. Pharmaceutical aspects of salt and cocrystal forms of APIs and characterization challenges. *Adv. Drug Delivery Rev.* **2017**, *117*, 86−110.
(17) Yamashita, H.; Hirakura, Y.; Yuda, M.; Teramura, T.; Terada, K. Detection of cocrystal formation based on binary phase diagrams using thermal analysis. *Pharm. Res.* **2013**, *30*, 70−80.
(18) Childs, S. L.; Hardcastle, K. I. Cocrystals of chlorzoxazone with carboxylic acids. *CrystEngComm* **2007**, *9*, 364−367.
(19) Nguyen, M.; Dougados, M.; Berdah, L.; Amor, B. Diacerhein in the treatment of osteoarthritis of the hip. *Arthritis Rheum.* **1994**, *37*, 529−536.
(20) Nicolas, P.; Tod, M.; Padoin, C.; Petitjean, O. Clinical pharmacokinetics of diacerein. *Clin. Pharmacokinet.* **1998**, *35*, 347−359.
(21) Tamura, T.; Shirai, T.; Kosaka, N.; Ohmori, K.; Takafumi, N. Pharmacological studies of diacerein in animal models of inflammation, arthritis and bone resorption. *Eur. J. Pharmacol.* **2002**, *448*, 81−87.
(22) Elsayed, I.; Abdelbary, A. A.; Elshafeey, A. H. Nanosizing of a poorly soluble drug: technique optimization, factorial analysis, and pharmacokinetic study in healthy human volunteers. *Int. J. Nanomed.* **2014**, *9*, 2943−2953.
(23) Batt, D. K.; Garala, K. C. Preparation and evaluation of inclusion complexes of diacerein with *β*-cyclodextrin and hydroxypropyl *β*-cyclodextrin. *J. Inclusion Phenom. Macrocyclic Chem.* **2013**, *77*, 471−481.
(24) El-Laithy, H. M.; Basalious, E. B.; El-Hoseiny, B. M.; Adel, M. M. Novel self-nanoemulsifying self-nanosuspension (SNESNS) for enhancing oral bioavailability of diacerein: simultaneous portal blood absorption and lymphatic delivery. *Int. J. Pharm.* **2015**, *490*, 146−154.
(25) Aggarwal, A. K.; Singh, S. Physicochemical characterization and dissolution study of solid dispersions of diacerein with polyethylene glycol 6000. *Drug Dev. Ind. Pharm.* **2011**, *37*, 1181−1191.
(26) Khan, M. I.; Madni, A.; Peltonen, L. Development and in-vitro characterization of sorbitan monolaurate and poloxamer 184 based niosomes for oral delivery of diacerein. *Eur. J. Pharm. Sci.* **2016**, *95*, 88−95.
(27) Malik, R.; Garg, T.; Goyal, A. K.; Rath, G. Diacerein-Loaded novel gastroretentive nanofiber system using PLLA: Development and in vitro characterization. *Artif. Cells, Nanomed., Biotechnol.* **2016**, *44*, 928−936.
(28) Jain, A.; Singh, S. K.; Singh, Y.; Singh, S. Development of lipid nanoparticles of diacerein, an antiosteoarthritic drug for enhancement in bioavailability and reduction in its side effects. *J. Biomed. Nanotechnol.* **2013**, *9*, 891−900.
(29) Childs, S. L.; Stahly, G. P.; Park, A. The salt - cocrystal continuum: the influence of crystal structure on ionization state. *Mol. Pharmaceutics* **2007**, *4*, 323−338.
(30) Raval, M. K.; Vaghela, P. D.; Vachhani, A. N.; Sheth, N. R. Role of excipients in the crystallization of Albendazole. *Adv. Powder Technol.* **2015**, *26*, 1102−1115.
(31) Patel, R. D.; Raval, M. K.; Pethani, T. M.; Sheth, N. R. Influence of eutectic mixture as a multi-component system in the improvement of physicomechanical and pharmacokinetic properties of diacerein. *Adv. Powder Technol.* **2020**, *31*, 1441−1456.
(32) Denny, P. J. Compaction equations: a comparison of the Heckel and Kawakita equations. *Powder Technol.* **2002**, *127*, 162−172.
(33) Fell, J. T.; Newton, J. M. Determination of tablet strength by the diametral-compression test. *J. Pharm. Sci.* **1970**, *59*, 688−691.
(34) Barot, B. S.; Parejiya, P. B.; Patel, T. M.; Parikh, R. K.; Gohel, M. C. Compactibility improvement of metformin hydrochloride by crystallization technique. *Adv. Powder Technol.* **2012**, *23*, 814−823.
(35) Wells, J. In *Pharmaceutics: The Science of Dosage Forms Design*, 2nd ed.; Aulton, M., Ed.; Churchill Livingstone: London, 2001; pp 197−210.
(36) *Indian Pharmacopoeia*; Government of India, Ministry of Health & Family Welfare: New Delhi, India, 2010; Vol. *III*, pp 1191−1193.
(37) Anderson, N. H.; Bauer, M.; Boussac, N.; Khan-Malek, R.; Munden, P.; Sardaro, M. An evaluation of fit factors and dissolution efficiency for the comparison of in vitro dissolution profiles. *J. Pharm. Biomed. Anal.* **1998**, *17*, 811−822.
(38) Tamura, T.; Shirai, T.; Kosaka, N.; Ohmori, K.; Takafumi, N. Pharmacological studies of diacerein in animal models of inflammation, arthritis and bone resorption. *Eur. J. Pharmacol.* **2002**, *448*, 81−87.
(39) Thenge, R. R.; Patond, V. B.; Ajmire, P. V.; Barde, L. N.; Mahajan, N. M.; Tekade, N. P. Preparation and characterization of co-crystals of diacerein. *Indones. J. Pharm.* **2017**, *28*, 34.
(40) Tomar, S.; Chakraborti, S.; Jindal, A.; Grewal, M. K.; Chadha, R. Cocrystals of diacerein: Towards the development of improved biopharmaceutical parameters. *Int. J. Pharm.* **2020**, *574*, 118942.
(41) Chun, N. H.; Wang, I. C.; Lee, M. J.; Jung, Y. T.; Lee, S.; Kim, W. S.; Choi, G. J. Characteristics of indomethacin-saccharin (IMC-SAC) co-crystals prepared by an anti-solvent crystallization process. *Eur. J. Pharm. Biopharm.* **2013**, *85*, 854−861.
(42) Kaur, R.; Gautam, R.; Cherukuvada, S.; Guru Row, T. N. Do carboximide-carboxylic acid combinations form co-crystals? The role of hydroxyl substitution on the formation of co-crystals and eutectics. *IUCrJ* **2015**, *2*, 341−351.
(43) Cherukuvada, S.; Guru Row, T. N. Comprehending the formation of eutectics and cocrystals in terms of design and their structural interrelationships. *Cryst. Growth Des.* **2014**, *14*, 4187−4198.
(44) Avula, S. G.; Alexander, K.; Riga, A. Thermal analytical characterization of mixtures of antipsychotic drugs with various excipients for improved drug delivery. *J. Therm. Anal. Calorim.* **2016**, *123*, 1981−1992.
(45) Bambagiotti-Alberti, M.; Bartolucci, G.; Bruni, B.; Coran, S. A.; Di Vaira, M. Physico-chemical and structural characterization of diacerhein. *J. Pharm. Biomed. Anal.* **2009**, *49*, 1065−1069.
(46) Raval, M. K.; Sorathiya, K. R.; Chauhan, N. P.; Patel, J. M.; Parikh, R. K.; Sheth, N. R. Influence of polymers/excipients on development of agglomerated crystals of secnidazole by crystallo-co-agglomeration technique to improve processability. *Drug Dev. Ind. Pharm.* **2013**, *39*, 437−446.
(47) Nie, B.; Stutzman, J.; Xie, A. A vibrational spectral maker for probing the hydrogen-bonding status of protonated Asp and Glu residues. *Biophys. J.* **2005**, *88*, 2833−2847.
(48) *ICH Harmonized Tripartite Guideline: Validation of Analytical Procedures: Text and Methodology Q2 (R1)*. International Conference on Harmonization, Geneva, Switzerland, November 2005. http://www.ich.org/fileadmin/Public_web_Site/ICH_Products/Guidelines/Quality/Q2_R1/Step4/Q2_R1_Guideline.pdf (accessed 2020-03-31).


https://dx.doi.org/10.1021/acs.oprd.0c00298
*Org. Process Res. Dev.* 2021, 25, 384−394

(49) Shah, P. P.; Mashru, R. C. Development and evaluation of artemether taste masked rapid disintegrating tablets with improved dissolution using solid dispersion technique. *AAPS PharmSciTech* **2008**, *9*, 494−500.
(50) Li, Q.; Rudolph, V.; Weigl, B.; Earl, A. Interparticle van der Waals force in powder flowability and compactibility. *Int. J. Pharm.* **2004**, *280*, 77−93.
(51) Wells, J. I. *Pharmaceutical Preformulation: The Physicochemical Properties of Drug Substances*; Ellis Horwood: Chichester, U.K., 1988.
(52) Kawashima, Y.; Imai, M.; Takeuchi, H.; Yamamoto, H.; Kamiya, K.; Hino, T. Improved flowability and compactibility of spherically agglomerated crystals of ascorbic acid for direct tableting designed by spherical crystallization process. *Powder Technol.* **2003**, *130*, 283−289.
(53) Ranjan, S.; Devarapalli, R.; Kundu, S.; Vangala, V. R.; Ghosh, A.; Reddy, C. M. Three new hydrochlorothiazide cocrystals: structural analyses and solubility studies. *J. Mol. Struct.* **2017**, *1133*, 405−410.
(54) Smith, A.; Kavuru, P.; Wojtas, L.; Zaworotko, M.; Shytle, R. Cocrystals of quercetin with improved solubility and oral bioavailability. *Mol. Pharmaceutics* **2011**, *8*, 1867−1876.
(55) Patel, R. D.; Raval, M. K.; Sheth, N. R. Formation of Diacerein - fumaric acid eutectic as a multi-component system for the functionality enhancement. *J. Drug Delivery Sci. Technol.* **2020**, *58*, 101562.


https://dx.doi.org/10.1021/acs.oprd.0c00298
*Org. Process Res. Dev.* 2021, 25, 384−394